Accepted Manuscript online: 2023-02-16 Article published online: 2023-03-01

A Flexible Aromatic Amphiphilic Trication for the Solubilization of Hydrophobic Organic Semiconductors in Water

Soujanya H. Goudar[a]
Srinu Kotha[a]
Manya Pal[a]
Dhiraj S. Ingle[a]
Kotagiri Venkata Rao* [a]

[a] Department of Chemistry, Indian Institute of Technology Hyderabad, Kandi, Sangareddy, Telangana 502285, India
* kvrao@chy.iith.ac.in

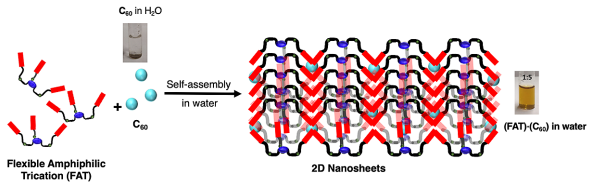

Received: 30.11.2022
Accepted after revision: 16.02.2023
DOI: 10.1055/a-2037-2786; Art ID: OM-2022-11-0050-OA

Abstract Amphiphiles are widely explored for the solubilization of various hydrophobic molecules especially drugs in water. Recently, aromatic amphiphiles emerged as a new class of molecules for the solubilization of hydrophobic organic semiconductors in water. However, the synthesis of these systems involves several steps and often requires the use of expensive metal catalysts. Here we describe the design and synthesis of a new type of flexible aromatic amphiphilic trication (FAT) and its application for solubilization of hydrophobic organic semiconductors in water. FAT has been synthesized in two steps without the use of any expensive metal catalysts. We observed that FAT self-assembles in water into bilayer two-dimensional (2D) nanosheets composed of hydrophobic naphthalimide units. FAT is found to be effective for the solubilization of various hydrophobic organic semiconductors such as perylene, perylene diimide and C_{60} in water by encapsulating them into its hydrophobic domains. Moreover, FAT was also explored for the solubilization of a 2D conjugated ladder polymer, TQBQ (triquinoxalinylene and benzoquinone), in water.

Key words: amphiphiles, host–guest chemistry, self-assembly, 2D nanosheets

Introduction

Amphiphiles[1–3] are the molecules that can self-assemble into many different types of nanostructures, such as micelles,[4,5] vesicles,[6,7] nanotubes and nanofibers.[8–10] When taken in water, the hydrophilic portion of the amphiphilic molecules preferentially interacts with the water, whereas the hydrophobic domain hides from water and creates hydrophobic domains or cavities. As a result, amphiphilic self-assembly in water is widely explored for drug delivery applications.[11–13] In the case of small molecules, three major types of amphiphilic designs such as oligoether,[14] peptide[15] and ionic[16] amphiphiles are widely explored. Over other types of molecular designs for self-assembly, amphiphiles are environmentally benign as water is used as a medium for self-assembly. In the beginning, amphiphiles having mainly hydrocarbon chains as the hydrophobic part are explored for self-assembly. Later, this design was extended to organic semiconducting π-systems to afford a novel class of nanostructures with tunable optoelectronic functions.[17–21] For example, Aida et al. synthesized semiconducting nanotubes using amphiphilic self-assembly of hexabenzocoronenes.[22] George et al. synthesized high-aspect ratio supramolecular nanofibers via ionic charge-transfer amphiphiles.[23] Recently, Stupp et al. explored perylene imide-based amphiphilic designs for water splitting applications.[24] Very recently, we reported that amphiphilic ionic π-systems undergo supramolecular depolymerization in the mixture of two poor solvents owing to segregation of water and amphiphilic organic solvent around the ionic π-system.[25]

In recent years, aromatic amphiphiles also have been explored for host–guest interactions in water.[26] Compared to conventional amphiphiles, aromatic amphiphiles are composed of hydrophobic pockets or cavities of π-systems. As a result, they can solubilize hydrophobic π-systems in water much better than conventional surfactant amphiphiles owing to the strong π–π interactions.[26] For this purpose, bent π-systems are preferred over linear π-systems. Yoshizawa et al. first developed an aromatic amphiphile having bent anthracene units which can efficiently encapsulate various hydrophobic π-systems.[27] Recently, they have also synthesized the bent pentacene-based aromatic micelle which can encapsulate perylene bisimide dyes and graphene nanosheets in water.[28] Compared to rigid metal organic cages,[29–31] small-molecule-based aromatic amphiphiles have several advantages like flexible size and high solubility for host–guest interactions in water. However, the currently known aromatic amphiphiles require multi-step synthesis. Hence, identifying new aromatic amphiphiles that are easily accessible with efficient host–guest interactions in water is important.

Here we report the design and synthesis of a naphthalimide-based flexible amphiphilic trication (**FAT**) for the solubilization of hydrophobic π-systems in water (Scheme 1). Importantly, **FAT** is synthesized in two steps from commercially available materials without the use of any expensive metal catalysts. Due to the presence of three ammonium cations, **FAT** is easily soluble in water and self-assembles into two-dimensional (2D) nanosheets having hydrophobic cavities composed of naphthalimides. Interestingly, these 2D nanosheets effectively solubilize various hydrophobic π-systems such as perylene, perylene diimide (PDI) and fullerene C_{60} in water which are otherwise not soluble. Moreover, we also utilized **FAT** to solubilize a 2D semiconducting organic polymer in water.

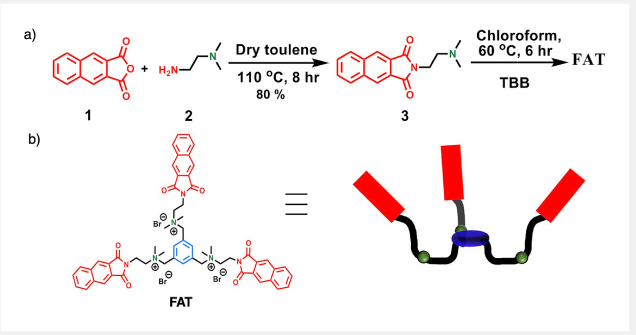

Scheme 1 a) Scheme for the synthesis of **FAT**. b) Schematic representation of **FAT** molecular structure.

Results and Discussion

Molecular design and synthesis: The molecular structure of **FAT** is shown in Scheme 1. In **FAT**, naphthalimide acts as a hydrophobic π-surface and three of these are covalently linked to the central benzene ring via three ammonium cations. **FAT** is synthesized in two steps. In the first step, 2,3-napthalene dicarboxylic anhydride **1** is reacted with *N,N*-dimethyl ethylene diamine to afford monoimide **3** in 80% yield. **3** is then reacted with 1,3,5-tris(bromomethyl) benzene (**TBB**) **4** to afford **FAT** in high yield, 87%. The formation of **FAT** has been confirmed by the ^{1}H NMR and ^{13}C NMR spectroscopy, HRMS, infrared (IR) spectroscopy and melting point (Figures S1 – S4). The optical properties of **FAT** are studied using UV-Vis and fluorescence spectroscopy. The self-assembled morphology of **FAT** is characterized using field-emission scanning electron microscopy (FE-SEM), atomic force microscopy (AFM) and transmission electron microscopy (TEM).

FAT is molecularly soluble in DMSO and self-assembles in water. In DMSO at 0.3 mM, **FAT** shows sharp and vibrationally resolved absorption peaks between 200 to 380 nm with two sets of absorption peaks centered at 270 and 361 nm (Figure 1a). Under similar conditions in water, **FAT** shows broad absorption peaks with a red-shift at a higher wavelength peak from 361 to 370 nm (Figure 1a). In the monomeric form in DMSO, **FAT** shows emission in the range of 365 to 450 nm with the emission maximum at 401 nm (Figure 1b). Compared to DMSO, the emission spectrum is relatively broad and red-shifted from 401 to 435 nm (Figure 1b). Interestingly **FAT** shows slight enhancement in the emission when taken in water. Since **FAT** is flexible in nature, the free rotation of naphthalimide units in good solvents like DMSO results in weak fluorescence. However, in water due to the rigidification and restricted motion of naphthalimide units upon self-assembly, fluorescence enhancement was observed.[32–34] The red-shift and enhancement in fluorescence emission are further evidenced from the solution photographs under UV light (Figure 1c). These observations indicate the presence of π–π stacking interactions in the self-assembly of **FAT** molecules. We have further probed the self-assembly of **FAT** using ^{1}H NMR studies in DMSO-d_6 and D_2O (Figure 1f). A 0.3 mM solution of **FAT** in DMSO-d_6 shows sharp signals in the aromatic region from 8.57 to 7.75 ppm. On the other hand, in D_2O the aromatic signals became broad, and the region is significantly upfield-shifted from 8.12 to 7.40 ppm. This is due to the shielding effect of aromatic systems with each other as a result of π–π stacking interactions.[35,36] These observations further indicate that **FAT** is going to self-assemble through π–π stacking interactions in D_2O, whereas in DMSO-d_6 they exist as isolated molecules.

To know the morphology of self-assembled aggregates of **FAT**, 0.3 mM aqueous solution of **FAT** is spin-coated on silicon wafer and dried under vacuum. When visualized these samples using FE-SEM (Figure 1d), a 2D nanosheet like morphology was observed, which is further supported by TEM and AFM measurements (Figures 1e and S9). From the AFM images, the height of a single sheet is found to be nearly 2.5 nm (Figure S9). Based on these observations, we have proposed the bilayer molecular packing of **FAT** molecules in 2D sheets where naphthalimides interact together to form hydrophobic cavities and benzyl ammonium groups are exposed to water (Figure 1g). However, no peaks in the low angle in powder X-ray diffraction (PXRD) were observed for **FAT** (Figure S11). This indicates the absence of a long-range 2D crystalline order for **FAT** molecules in nanosheets. The peak observed at 27.8° (2θ) corresponding to a *d*-spacing of 0.32 nm indicates the presence of π–π stacking interactions between **FAT** molecules in the nanosheets (Figure S11). Later we also conducted concentration-dependent studies in water from 0.3 to 1.5 mM (Figure S10). Interestingly, with increasing concentration, the ratio of absorption band in the 300 – 400 nm gradually increased and at 1.5 mM, the absorbance was slightly higher than the band in the 200 – 300 nm region. However, no further shifts were observed in the corresponding emission spectra. The morphol-

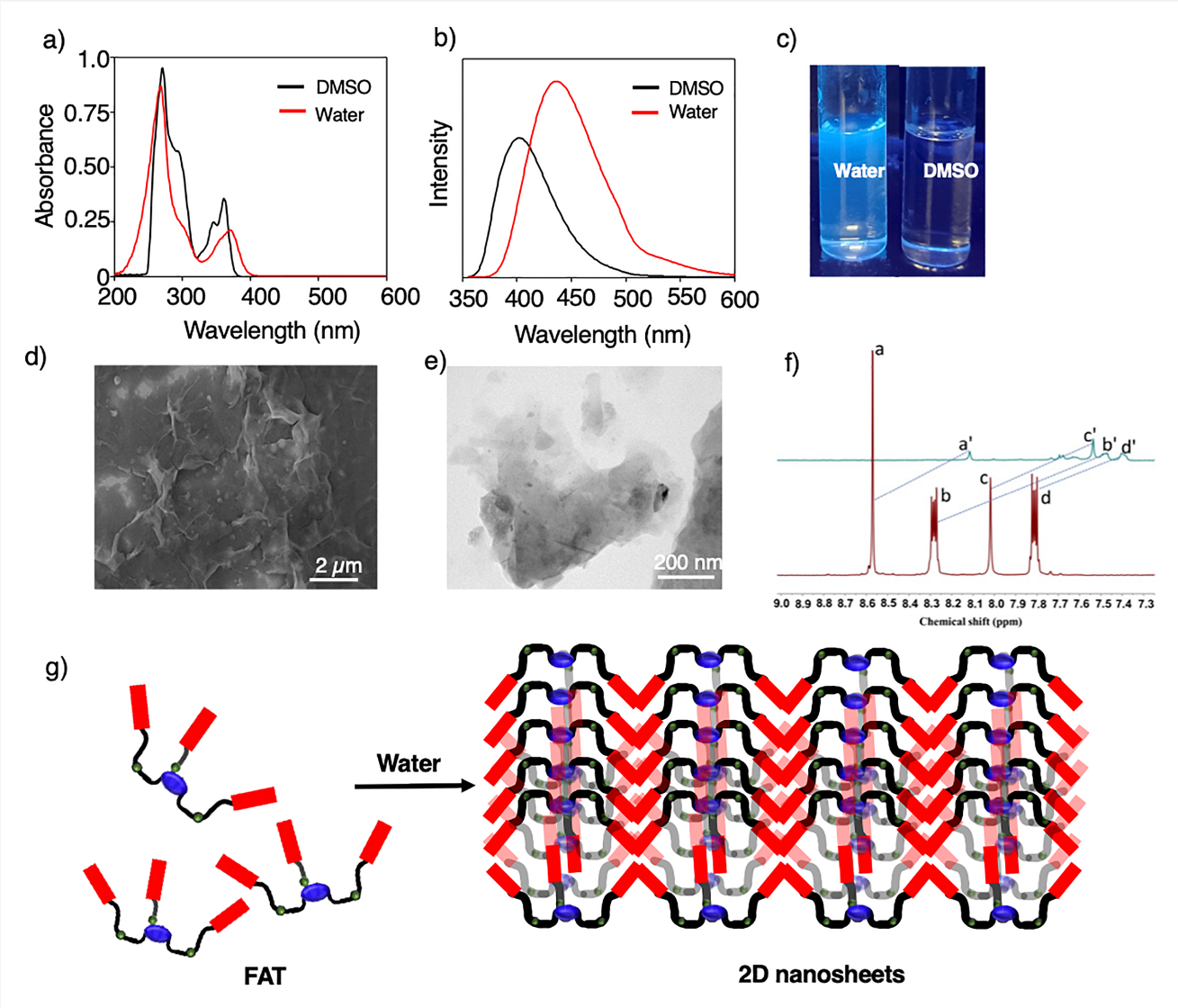

Figure 1 a) Electronic absorption spectra and b) emission spectra (λ_{ex} = 345 nm) of **FAT** molecule in DMSO and water at 0.3 mM concentration. c) Photographs of **FAT** in water and DMSO under UV light. d) SEM and e) TEM images of **FAT** at 0.3 mM concentration in water. f) ^{1}H NMR spectra of the aromatic region of **FAT** in DMSO-d_6 and D_2O at 0.3 mM concentration. g) Schematic representation of 2D self-assembly of **FAT** in the water.

ogy of **FAT** at higher concentrations indicates the presence of large and thick sheets probably due to further stacking of 2D nanosheets (Figure S11).

Host–Guest Studies

Since **FAT** forms 2D nanosheets in water and is composed of three aromatic hydrophobic naphthalimide panels, we explored it further for the solubilization of various hydrophobic organic semiconducting guest molecules in water. For this purpose, we selected perylene, PDI, C_{60} and a 2D polymer as guest molecules. First, we investigated the solubilization of perylene in water with the aid of **FAT** (Figure 2). Due to its hydrophobic nature, perylene is not soluble in water but readily soluble in chloroform (Figures 2a and S12). In chloroform, perylene shows major vibrationally resolved absorption peaks from 300 to 450 nm (Figure S12). However, in water perylene alone is not soluble as evidenced by the absence of any absorption peaks from 300 to 450 nm in water (Figures 2b and S12). This is also further evidenced from the photograph of perylene in water (Figure 2a). Interestingly, when **FAT** and perylene were mixed in water, the color of the solution turned yellow indi-

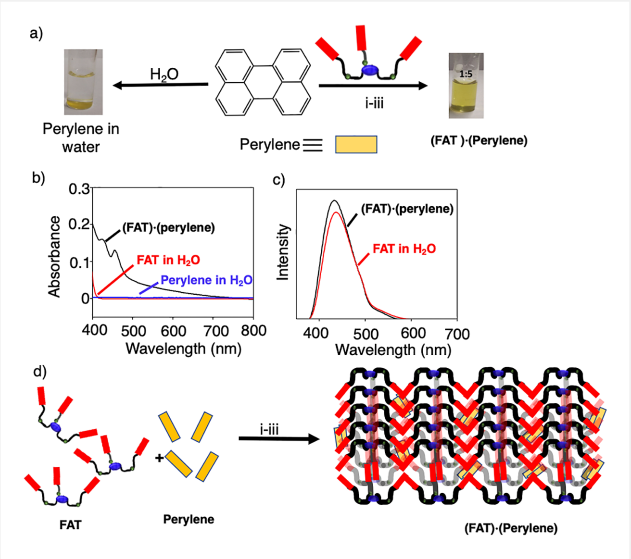

Figure 2 a) Photograph of perylene alone in water (left) and encapsulation of perylene by **FAT** (1.5 mM) molecule in water and the photograph of resultant solution of (**FAT**)·(perylene) complex (right). Procedures: i) manual grinding (5 min), ii) water addition, and iii) centrifugation. b) Electronic absorption spectra of **FAT** (1.5 mM), perylene and (**FAT**)·(perylene) complex in water. c) fluorescence spectra (λ_{ex} = 370 nm) of **FAT** (1.5 mM), perylene and (**FAT**)·(perylene) complex in water. The fluorescence intensity was corrected for the absorbance. d) Schematic representation of formation of (**FAT**)·(perylene) complex.

cating the solubilization of perylene in water in the presence of **FAT** (Figure 2a). In a typical experimental procedure, 5 equiv. of **FAT** (1.5 mM) are mixed with 1 equiv. of perylene (0.3 mM) in the solid state followed by the addition of water. Next, we employed grinding and ultrasonication to have a proper mixing of **FAT** and perylene. The resultant solution was centrifuged to remove any insoluble perylene molecules. The yellow color of the obtained (**FAT**)·(perylene) solution clearly indicates the presence of perylene in water. To confirm the presence of perylene in water, we recorded the absorption spectra of (**FAT**)·(perylene) solution. The absorbance of **FAT** alone in water ends around ~410 nm, whereas the (**FAT**)·(perylene) aqueous solution showed the absorbance till 700 nm (Figure 2b). This clearly indicates the solubilization of perylene in water by **FAT** as perylene alone in water does not display any absorbance from 400 to 700 nm region. The possible driving forces for the solubilization of perylene in water by **FAT** are hydrophobic and π–π stacking between naphthalimide and perylene. For **FAT** alone in water at 1.5 mM, the absorbance of a longer wavelength band is slightly higher than that of a shorter wavelength band (Figure S10). However, upon perylene encapsulation, the absorbance of the absorption band centered at 267 nm is higher than the band at 370 nm (Figure S13). These observations further support the perylene (guest) encapsulation in **FAT** assemblies as it affects the stacking of host (**FAT**) molecules due to π–π stacking interactions between the guest and the host in the host–guest complex. As a result, the fluorescence intensity of (**FAT**)·(perylene) is slightly higher than **FAT** alone (Figure 2c). In chloroform, perylene is molecularly soluble without any π–π stacking as evidenced by the higher absorbance of 0 – 0 transition than 0 – 1 transition (Figure S12). However, the absorption spectra of perylene in (**FAT**)·(perylene) aqueous solution show the higher absorbance for the 0 – 1 transition than the 0 – 0 transition and the appearance of a new broad absorption band from 500 to 700 nm (Figure 2b). These observations clearly indicate the presence of perylene aggregates in (**FAT**)·(perylene) aqueous solution (Figure 2d).

To understand the importance of **FAT**, we have also prepared flexible amphiphilic dictation (**FAD**) and compared their water solubilizing ability toward perylene (see section 1.2 in the Supporting Information). The same protocol was followed to prepare the host–guest complex of (**FAD**)·(perylene). Even with 7 equiv. of **FAD**, the absorbance of perylene in water is ~2.5 times lower compared to (**FAT**)·(perylene) solution (Figure S14). This is also further evident from the less intense yellow-colored solution (Figure S14). These observations indicate that the more the hydrophobic aromatic units, the higher is the guest encapsulation behavior. Moreover, the tripodal structure of **FAT** also might play a more important role than the linear structure of **FAD** for efficient capture of guest molecules in water as the former can create better hydrophobic pockets than the later.

Further we explored the host characteristics of **FAT** with PDI molecule. PDIs are an important class of organic dyes which are frequently employed as supramolecular building blocks.[37,38] The planar core of PDI dyes aggregate via π-stacking interactions and exhibit strong absorption bands in the visible region (Figure 3). 3,5-Diisopropylphenyl-substituted PDI is insoluble in water and shows good solubility in $CHCl_3$ (Figure S12). Like perylene, **FAT** could readily solubilize PDI in water at room temperature upon encapsulation (Figure 3a). The same protocol was followed for PDI also by mixing it with 5 equiv. of **FAT**. After sequential water addition and centrifugation, a host–guest complex (**FAT**)·(PDI) was formed as a clear, red aqueous solution (Figure 3a). The formation of the host–guest complex was further confirmed by measuring UV-Vis spectra. The appearance of sharp intense bands in the range of 400 – 600 nm confirmed the successful formation of the host–guest complex between **FAT** and **PDI** (Figure 3b). Similar to (**FAT**)·(perylene), the absorbance of **FAT** at 267 nm is higher than the band at 371 nm upon encapsulation of PDI (Figure S13). Moreover, the fluorescence intensity of **FAT** in (**FAT**)·(PDI) complex is slightly higher than **FAT** alone like in (**FAT**)·(perylene) (Figure 3c). Since PDI is an electron acceptor, fluorescence quenching of **FAT** is expected after PDI encapsulation due to charge-transfer interactions. Instead, fluorescence enhancement of **FAT**

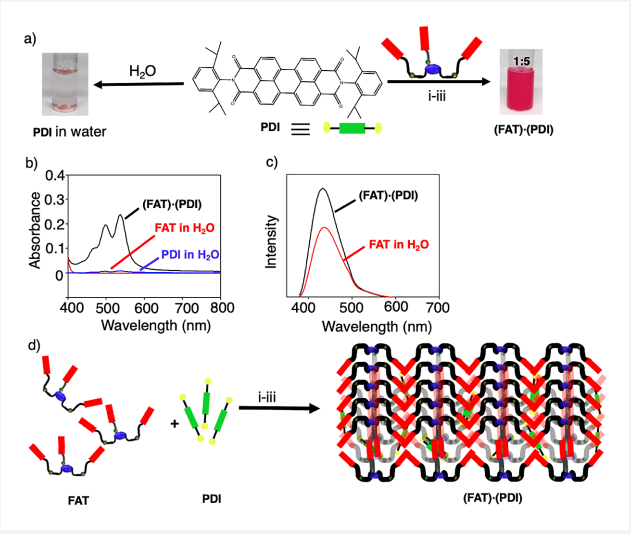

Figure 3 a) Photograph of PDI in water (left) and encapsulation of PDI by **FAT** (1.5 mM) molecule in water and photograph of resultant solution of (**FAT**)·(PDI) complex and perylene in water. Procedures: i) manual grinding (5 min), ii) water addition, and iii) centrifugation. b) Electronic absorption spectra of PDI, **FAT** and (**FAT**)·(PDI) complex in water. c) fluorescence spectra of **FAT** and (**FAT**)·(PDI) complex in water (λ_{ex} = 370 nm). The fluorescence intensity was corrected for the absorbance. d) Schematic representation of formation of (**FAT**)·(PDI) complex in water.

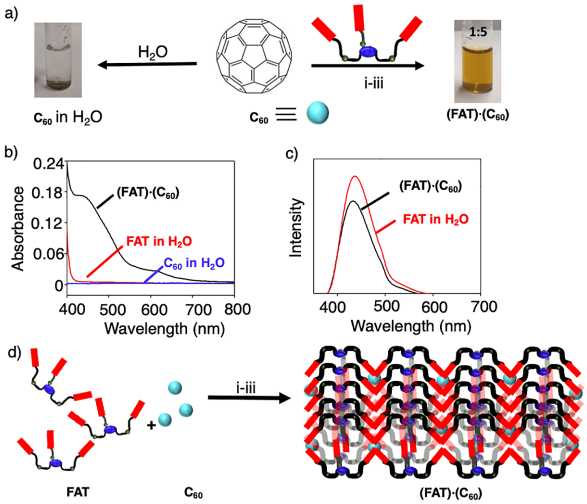

Figure 4 a) Photograph of C_{60} (left) and encapsulation of C_{60} by **FAT** molecule in water and photograph of resultant solutions of (**FAT**)·(C_{60}) complex in water. Procedures: i) manual grinding (5 min), ii) water addition, and iii) centrifugation. b) Electronic absorption spectra of **FAT** (1.5 mM), C_{60} and (**FAT**)·(C_{60}) complex in water. c) Fluorescence emission spectra of **FAT** and (**FAT**)·(C_{60}) complex in water (λ_{ex} = 370 nm). The fluorescence intensity was corrected for the absorbance. d) Schematic representation of formation of (**FAT**)·(C_{60}) complex in water.

is observed. This could be due to the bulky substituents on PDI which prevent the π–π stacking interactions between naphthalimide of **FAT** and PDI although encapsulation takes place through hydrophobic interactions. As a result, charge transfer interactions between **FAT** and PDI are suppressed. The increase in the emission of **FAT** after encapsulation of PDI could be due to change of molecular packing as evidenced by the change of ratio of absorptions bands centered at 267 and at 370 nm before and after encapsulation like in the case of (**FAT**)·(perylene) complex (Figures S10 and S13). To understand the state of PDI in (**FAT**)·(PDI) complex, we analysed the ratio of 0–0 transition to 0–1 transition absorbance of PDI in chloroform and in (**FAT**)·(PDI) complex in water. In chloroform, the ratio of 0–0 to 0–1 transition is 1.64, indicating the isolated nature of PDIs without any π–π stacking interactions (Figure S12). However, in (**FAT**)·(PDI) complex in water, ratio of 0–0 to 0–1 transition is reduced to 1.12 (Figure 3b). This indicates the presence of both isolated and assembled PDIs in (**FAT**)·(PDI) complex in water (Figure 3d).

Inspired by the solubilization of perylene and PDI by **FAT** in water, we next explored one of the well-known hydrophobic organic semiconductors, fullerene, C_{60}.[39,40] Owing to the rigid aromatic buckyball structure, C_{60} alone is soluble only in aromatic solvents like toluene and insoluble in water (Figures 4a and S12). Interestingly, when C_{60} is mixed with **FAT** in 1 : 5 molar ratio using the procedure followed for perylene and PDI, the resultant aqueous solution appears brown in colour, indicating the solubilization of C_{60} in water (Figure 4a). This is further supported by the appearance of an absorption band in the range 400–550 nm in the UV-Vis spectrum, which is assignable to the encapsulated C_{60} (Figure 4b). In toluene, C_{60} (0.3 mM) shows vibrationally resolved sharp absorption peaks due to the absence of any π–π interactions among C_{60} molecules (Figure S12). On the other hand, in the (**FAT**)·(C_{60}) complex in water, C_{60} shows broad absorption spectra from 400 to 700 nm (Figure 4b). This could be due to the aggregation of C_{60} molecules after encapsulation in **FAT** 2D nanosheets in water (Figure 4d). In contrast to perylene, the encapsulation of C_{60} slightly reduces the fluorescence of FAT probably due to charge-transfer interactions as C_{60} is a strong electron acceptor (Figure 4c).

The successful solubilization of one-dimensional small molecules like perylene and PDI and zero-dimensional C_{60} has prompted us to explore the solubilization of a triquinoxalinylene and benzoquinone (TQBQ)-derived 2D conjugated ladder polymer in water.[41] TQBQ is a 2D-conjugated covalent organic polymer with high-performance energy storage properties.[41] Like TQBQ, many 2D organic polymers such as covalent organic frameworks show interesting gas storage, optoelectronic and energy storage functions.[42] However,

owing to the insolubility in many common organic solvents and water, these materials are difficult to process, which severally limits them for various applications. Interestingly, when **FAT** (5 mg) and TQBQ (1 mg) polymer were mixed together followed by the addition of water and centrifugation resulted in a black coloured solution (Figure 5a). Since TQBQ alone is not soluble in water, the change of water colour to dark brown when **FAT** and TQBQ are taken together indicates the solubilization of TQBQ in water via the formation of (**FAT**)·(TQBQ) complex (Figure 5 d). The formation of the host–guest complex was further confirmed by UV absorption spectra (Figure 5b). The appearance of absorbance in the range of 400 – 850 nm in water clearly indicated the presence of TQBQ polymer (Figure 5b). The fluorescence intensity of **FAT** slightly decreased after TQBQ encapsulation, which could be due to charge-transfer interactions between **FAT** and TQBQ because of the electron-deficient nature of TQBQ like C_{60} (Figure 5c).

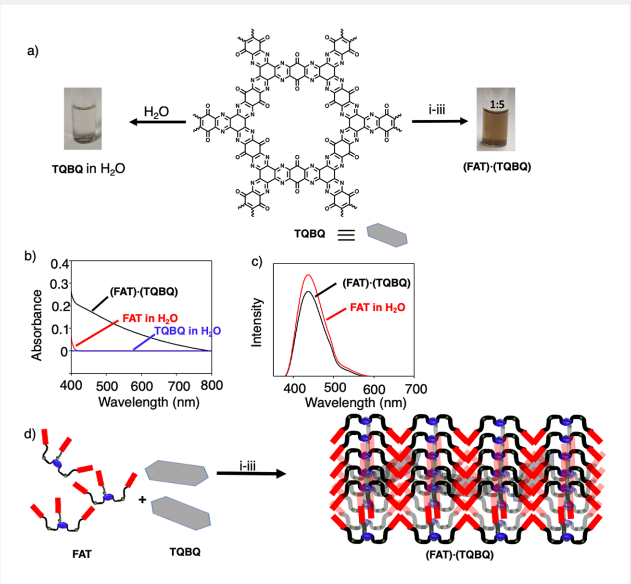

Figure 5 a) Photograph of TQBQ in water (left) and encapsulation of TQBQ by **FAT** molecule in water and photograph of resultant (**FAT**)·(TQBQ) complex and perylene in water. Procedures: i) manual grinding (5 min), ii) water addition, and iii) centrifugation. b) Electronic absorption spectra of **FTA** (1.5 mM), TQBQ and (**FAT**)·(TQBQ) complex in water. c) Fluorescence emission spectra of **FAT** and (**FAT**)·(TQBQ) complex in water (λ_{ex} = 370 nm). The fluorescence intensity was corrected for the absorbance. d) Schematic representation of formation of (**FAT**)·(TQBQ) complex.

Conclusions

In conclusion, we have designed and synthesised a tripodal-shaped flexible and amphiphilic naphthalimide trication (**FAT**). **FAT** is easily synthesized in two steps from commercially available materials. **FAT** is readily soluble in water and self-assembles into 2D bilayer nanosheets in water with segregated hydrophobic and hydrophilic domains. Moreover, **FAT** effectively solubilizes various water-insoluble hydrophobic organic semiconducting small molecules such as perylene, PDI and C_{60}. Additionally, **FAT** is also effective to solubilize a 2D-conjugated organic ladder polymer, TQBQ. Hydrophobic, π–π stacking and charge-transfer interactions are responsible for the solubilization of hydrophobic organic semiconductors in water by **FAT**. We believe that the easy synthesis of **FAT** allows us to extend this molecular design to various other monoimide π-systems to explore host–guest interactions and optoelectronic functions in water.

Experimental Section

Reagents were purchased at reagent grade from commercial sources and used without further purification. ^{1}H and ^{13}C NMR spectra were recorded on a Bruker 400 MHz spectrometer at 295 K, respectively, where chemical shifts (δ in ppm) were determined by fixing the solvent peak position. High-resolution mass spectra were recorded using electrospray ionization and Q-TOF techniques. FT-IR spectra were recorded using a JASCO model FTIR-4600. Melting point was recorded using a Tempo and Mettler FP1 melting point apparatus in capillary tubes. Electronic absorption spectra were recorded using a JASCO model V-770 UV-Vis-NIR spectrophotometer in a screw-capped quartz cell of 1 mm or 10 mm optical path length. Fluorescence spectra were recorded using a JASCO model FP-8300 spectrometer in a screw-capped quartz cell of 1 mm or 10 mm optical path length. SEM measurements were performed on a JEOL JIB4700F (FIB-SEM). TEM images were recorded using a transmission electron microscope (JEOL JEM 2100FX TEM, Japan) at the accelerating voltage of 200 kV. AFM images were recorded using Park (NX10). PXRD was recorded using Rigaku (Rigaku Ultima IV, Rigaku) with a Cu target [Cu Kα1 radiation (λ = 1.54 Å)] as a radiation source.

Procedures

Synthesis of FAT

2,3-Naphthalene dicarboxylic anhydride (**1**, 400 mg, 2.018 mmol) was taken in a 50 mL double-necked round bottom flask and 20 mL of dry toluene was added to it. To the stirred solution of anhydride and toluene, *N,N*-dimethylethaneamine (**2**, 533 mg, 6.05 mmol) was added dropwise for 5 min. After 8 h of reflux of the reaction mixture, a clear solution was obtained, which indicates the completion of the reaction, then the solvent was removed under reduced pressure. Compound **3** (433.23 mg, 1.61 mmol) was ob-

tained as white powder in 80% yield. This was carried out to the next step. Compound **3** (200 mg, 0.745 mmol) and 1,3,5-TBB (**4**, 44.35 mg, 0.124 mmol) were again taken in a 50 mL round bottom flask in 20 mL of chloroform and the reaction mixture was refluxed for 6 h. The obtained precipitate was filtered under reduced pressure and washed several times with chloroform. The final product was obtained as a white solid in 87% (693.16 mg, 0.596 mmol) yield. ^{1}H NMR (400 MHz, DMSO-d6) δ(ppm) = 8.57 (s, 6 H), 8.28 (dd, J = 6.1, 3.3 Hz, 6 H), 8.02 (s, 3 H), 7.81 (dd, J = 6.2, 3.3 Hz, 6 H), 4.82 (s, 6 H), 4.29 (t, J = 6.8 Hz, 6 H), 3.79 (t, J = 6.5 Hz, 6 H), 3.21 (s, 18 H). ^{13}C NMR δ(ppm) = 168.1, 139.5, 135.6, 130.8, 129.9, 128.1, 125.8, 65.6, 60.1, 50.0, 32.3. IR (KBr) ν cm^{-1} = 3406.6, 2960.2, 1765.6, 1387.5, 1108.0, 768.4, 540.9, 478.2. HRMS: m/z calculated for $[M + H]^{3+}$ is 307.1441, found 307.1419, m/z calculated for $[M + H]^{2+}$ is 501.1756, found 501.1717, and m/z calculated for $[M + H]^{1+}$ is 1081.2681, found 1081.2630. Melting point: 246 °C.

Funding Information

K.V.R. thanks Board of Research in Nuclear Sciences, India (Grant No. 58/14/04/2022-BRNS) for financial support. S.H.G. and S.K. thank the CSIR, India for the senior research fellowship. D.S.I. thanks Ministry of Education (MoE) for senior research fellowship.

Supporting Information

Supporting Information for this article is available online at https://doi.org/10.1055/a-2037-2786.

Conflict of Interest

The authors declare no conflict of interest.

References

(1) Lombardo, D.; Kiselev, M. A.; Magazù, S.; Calandra, P. *Adv. Condens. Matter Phys*. **2015**, *2015*, 151683.
(2) Chowdhury, S.; Rakshit, A.; Acharjee, A.; Saha, B. *ChemistrySelect* **2019**, *4*, 6978.
(3) Feast, G. C.; Lepitre, T.; Mulet, X.; Conn, C. E.; Hutt, O. E.; Savage, G. P.; Drummond, C. J. *Beilstein J. Org. Chem*. **2014**, *10*, 1578.
(4) Holder, S. J.; Sommerdijk, N. A. J. M. *Polym. Chem*. **2011**, *2*, 1018.
(5) Kimura, Y.; Ouchi, M.; Terashima, T. *Polym. Chem*. **2020**, *11*, 5156.
(6) Xing, P.; Sun, T.; Hao, A. *RSC Adv*. **2013**, *3*, 24776.
(7) Ogasawara, M.; Lin, X.; Kurata, H.; Ouchi, H.; Yamauchi, M.; Ohba, T.; Kajitani, T.; Fukushima, T.; Numata, M.; Nogami, R.; Adhikari, B.; Yagai, S. *Mater. Chem. Front*. **2018**, *2*, 171.
(8) Shimizu, T.; Masuda, M.; Minamikawa, H. *Chem. Rev*. **2005**, *105*, 1401.
(9) Hill, J. P.; Jin, W.; Kosaka, A.; Fukushima, T.; Ichihara, H.; Shimomura, T.; Ito, K.; Hashizume, T.; Ishii, N.; Aida, T. *Science*, **2004**, *304*, 1481.
(10) Liao, H. S.; Lin, J.; Liu, Y.; Huang, P.; Jin, A.; Chen, X. *Nanoscale* **2016**, *8*, 14814.
(11) Gupta, S.; Tyagi, R.; Parmar, V. S.; Sharma, S. K.; Haag, R. *Polymer* **2012**, *53*, 3053.
(12) Kwon, G. S.; Kataoka, K. *Adv. Drug Delivery Rev*. **2012**, *64*, 237.
(13) Song, Z.; Chen, X.; You, X.; Huang, K.; Dhinakar, A.; Gu, Z.; Wu, J. *Biomater. Sci*. **2017**, *5*, 2369.
(14) Rao, K. V.; George, S. J. *Org. Lett*. **2010**, *12*, 2656.
(15) Hendricks, M. P.; Sato, K.; Palmer, L. C.; Stupp, S. I. S. *Acc. Chem. Res*. **2017**, *50*, 2440.
(16) Hirohisa, N.; Koji, H.; Mayuko, I.; Ellen, B.; Mischa, B. *J. Am. Chem. Soc*. **2017**, *139*, 7677.
(17) Thirumalai, R.; Mukhopadhyay, R. D.; Praveen, V. K.; Ajayaghosh, A. *Sci. Rep*. **2015**, *5*, 09842.
(18) Ghosh, S.; Cherumukkil, S.; Suresh, C. H.; Ajayaghosh, A. *Adv. Mater*. **2017**, *29*, 1703783.
(19) Krieg, E.; Bastings, M. M. C.; Besenius, P.; Rybtchinski, B. *Chem. Rev*. **2016**, *116*, 2414.
(20) Rajdev, P.; Chakraborty, S.; Schmutz, M.; Mesini, P.; Ghosh, S. *Langmuir* **2017**, *33*, 4789.
(21) Rajdev, P.; Ghosh, S. *J. Phys. Chem. B* **2021**, *125*, 8981.
(22) Zhang, W.; Jin, W.; Fukushima, T.; Saeki, A.; Seki, S.; Aida, T. *Science*. **2011**, *334*, 340.
(23) Rao, K. V.; Jayaramulu, K.; Maji, T. K.; George, S. J. *Angew. Chem*. **2010**, *122*, 4314.
(24) Sai, H.; Erbas, A.; Dannenhoffer, A.; Huang, D.; Weingarten, A.; Siismets, E.; Jang, K.; Qu, K.; Palmer, L. C.; Olvera De La Cruz, M.; Stupp, S.I. *J. Mater. Chem. A*. **2020**, *8*, 158.
(25) Kotha, S.; Mabesoone, M. F. J.; Srideep, D.; Sahu, R.; Reddy, S. K.; Rao, K. V. *Angew. Chem. Int. Ed*. **2021**, *60*, 5459.
(26) Yoshizawa, M.; Catti, L. *Acc. Chem. Res*. **2019**, *52*, 2392.
(27) Kondo, K.; Suzuki, A.; Akita, M.; Yoshizawa, M. *Angew. Chem. Int. Ed*. **2013**, *52*, 2308.
(28) Ito, K.; Nishioka, T.; Akita, M.; Kuzume, A.; Yamamoto, K.; Yoshizawa, M. *Chem. Sci*. **2020**, *11*, 6752.
(29) Yazaki, K.; Akita, M.; Prusty, S.; Chand, D. K.; Kikuchi, T.; Sato, H.; Yoshizawa, M. *Nat. Commun*. **2017**, *8*, 15914.
(30) Yamashina, M.; Sartin, M. M.; Sei, Y.; Akita, M.; Takeuchi, S.; Tahara, T.; Yoshizawa, M. *J. Am. Chem. Soc*. **2015**, *137*, 9266.
(31) Kishi, N.; Akita, M.; Kamiya, M.; Hayashi, S.; Hsu, H.-F.; Yoshizawa, M. *J. Am. Chem. Soc*. **2013**, *135*, 12976.
(32) Mukherjee, S.; Thilagar, P. *Chem. Commun*. **2013**, *49*, 7292.
(33) Das, G.; Thirumalai, R.; Vedhanarayanan, B.; Praveen, V. K.; Ajayaghosh, A. *Adv. Opt. Mater*. **2020**, *8*, 2000173.
(34) Hong, Y.; Lam, J. W. Y.; Tang, B. Z. *Chem. Soc. Rev*. **2011**, *40*, 5361.
(35) Rao, K. V.; Jayaramulu, K.; Maji, T. K.; George, S. J. *Angew. Chem. Int. Ed*. **2010**, *49*, 4218.
(36) Parenti, F.; Tassinari, F.; Libertini, E.; Lanzi, M.; Mucci, A. *ACS Omega* **2017**, *2*, 5775.
(37) Würthner, F. *Chem. Commun*. **2004**, 1564.
(38) Wu, F.; Saha-mo, C. R.; Fimmel, B.; Ogi, S.; Leowanawat, P.; Schmidt, D. *Chem. Rev*. **2016**, *116*, 962.
(39) Prato, M. *J. Mater. Chem*. **1997**, *7*, 1097.
(40) Jia, L.; Chen, M.; Yang, S. *Mater. Chem. Front*. **2020**, *4*, 2256.
(41) Shi, R.; Liu, L.; Lu, Y.; Wang, C.; Li, Y.; Li, L.; Yan, Z.; Chen, J. *Nat. Commun*. **2020**, *11*, 178.
(42) Zhang, T.; Zhang, G.; Chen, L. *Acc. Chem. Res*. **2022**, *55*, 795.